

Splaying of Aliphatic Tails Plays a Central Role in Barrier Crossing During Liposome Fusion

Dina Mirjanian,^{†,§} Allison N. Dickey,[†] Jan H. Hoh,[‡] Thomas B. Woolf,[‡] and Mark J. Stevens*,[†]

Center for Integrated Nanotechnologies, Sandia National Laboratories, Albuquerque, New Mexico, Johns Hopkins University School of Medicine, Baltimore, Maryland

Received: June 15, 2010; Revised Manuscript Received: July 29, 2010

The fusion between two lipid bilayers involves crossing a complicated energy landscape. The limiting barrier in the process appears to be between two closely opposed bilayers and the intermediate state where the outer leaflets are fused. We have performed molecular dynamics simulations to characterize the free energy barrier for the fusion of two liposomes and to examine the molecular details of barrier crossing. To capture the slow dynamics of fusion, a model using coarse-grained representations of lipids was used. The fusion between pairs of liposomes was simulated for four systems: DPPC, DOPC, a 3:1 mixture of DPPC/DPPE, and an asymmetric lipid tail system in which one tail of DPPC was reduced to half the length (ASTail). The weighted histogram method was used to compute the free energy as a function of separation distance. The relative barrier heights for these systems was found to be ASTail \gg DPPC > DPPC/DPPE > DOPC, in agreement with experimental observations. Further, the free energy curves for all four can be overlaid on a single curve by plotting the free energy versus the surface separation (differing only in the point of fusion). These simulations also confirm that the two main contributions to the free energy barrier are the removal of water between the vesicles and the deformation of the vesicle. The most prominent molecular detail of barrier crossing in all cases examined was the splaying of lipid tails, where initially a single splayed lipid formed a bridge between the two outer leaflets that promotes additional lipid mixing between the vesicles and eventually leads to fusion. The tail splay appears to be closely connected to the energetics of the process. For example, the high barrier for the ASTail is the result of a smaller distance between terminal methyl groups in the splayed molecule. The shortening of this distance requires the liposomes to be closer together, which significantly increases the cost of water removal and bilayer deformation. Before tail splay can initiate fusion, contact must occur between a tail end and the external water. In isolated vesicles, the contact fraction is correlated to the fusogenicity difference between DPPC and DOPC. Moreover, for planar bilayers, the contact fraction is much lower for DPPC, which is consistent with its lack of fusion in giant vesicles. The simulation results show the key roles of lipid tail dynamics in governing the fusion energy landscape.

Introduction

The fusion of biological membranes is central to processes ranging from intracellular trafficking to exocytosis and infection by enveloped viruses.^{1–3} Although all of these processes require specific proteins to control and facilitate fusion, the idea that the physical chemistry of the underlying merger of lipid bilayers is similar in many, if not most cases, and has gained a broad following.⁴ As a consequence, liposomes produced *in vitro* under well-defined conditions have become a widely used model for understanding fundamental aspects of biological membrane fusion. Liposomes also have important technological applications as delivery vehicles for a variety of therapeutic and diagnostic agents that depend on fusion.⁵ Thus, there is significant interest in understanding the mechanisms of bilayer fusion in the liposome model. Experimental studies of liposome fusion over many years have provided significant insight into the role that various experimental parameters, such as temperature, liposome dimensions, and liposome composition, play in fusion as well as defining critical steps in the process. However,

the molecular details of the fusion between two lipid bilayers have largely resisted experimental elucidation.

The experimental studies in combination with theoretical models have led to the view that fusion proceeds along the following axis: the approach of two liposomes; the protrusion deformation of the lipid bilayer; the fusion of the outer leaflets of the liposomes (the stalk); the dilation and contact of inner leaflets; and finally, the fusion of the inner leaflets.^{6,7} The main barriers in this process are located between the close approach and formation of the stalk and likely depend significantly on the elastic energy of the membrane bending, including lipid tilt and the confinement and the repulsion associated with water between the membranes. Continuum calculations^{7,8} have suggested that the barrier at this step could be as high as 45 kT, although other approaches^{9–12} have produced barriers in the range 6–20 kT. With respect to the deformation of the bilayer, one proposed structure is the so-called nipple. The nipple is a small protrusion from the bilayer surface that has a very small radius of curvature, yielding a high barrier energy. In our own previous work, we have found that two liposomes brought into contact can form a flat contact region centered on the point of closest approach and that deformations that nucleate membrane fusion occur at the edge of this flat contact. In addition, recent simulations question aspects of the stalk model.¹¹

* Corresponding author. E-mail: msteve@sandia.gov.

[†] Sandia National Laboratories.

[‡] Johns Hopkins University School of Medicine.

[§] Present address: Molecular Foundry, Lawrence Berkeley National Laboratory, Berkeley, CA.

TABLE 1: Vesicle Diameters^a

	DPPC	PC/PE	DOPC	ASTail
D_h	129	129	135.8	120
D_t	136	136	144	130
D_o	156	156	162	146
D_f	132.5	131	138	122

^a D_h is calculated from the peak position in the outer leaflet head group. D_t is calculated from the position where the tail distribution goes to zero. D_o is calculated from the position where the outer head group distribution goes to zero. Units are in Å.

Simulations of membrane fusion offer an approach to characterize details of bilayer fusion in molecular detail with a temporal resolution that is short relative to the kinetics of the process.^{9,11–18} The development of coarse-grained lipid models represented a significant breakthrough which permitted bilayer systems of useful dimensions to be simulated over many milliseconds or more. These coarse-grained models for lipid bilayers have been shown to capture many known behaviors and properties of bilayers, which provide some level of confidence that they can be used to understand unknown aspects of bilayer dynamics.^{19–23} We have exploited these advantages to perform simulations of fusion in which all molecules are explicitly represented and to study the dynamics of fusion between two liposomes in water.¹⁶ These simulations reveal that the splaying of lipid tails at the initial point of fusion provides a mechanism for crossing the space between the bilayers and producing outer leaflet fusion.

Here, we extend the previous studies on the coarse-grained liposome model by using free energy methods to estimate the height of the barrier to lipid bilayer fusion. The free energy computations are complemented by the characterization of the molecular details of barrier crossing using the molecular dynamics trajectories. The energy barrier is estimated by computing the potential of mean force (PMF) to bring two well-separated vesicles together to the point of initial fusion. Thus, our reaction coordinate for the fusion process is the distance between the centers of mass of two vesicles. We also extend the previous work by studying the effect of tail type on fusion initiation. We treat four different lipid compositions: DPPC, DOPC, an asymmetric tail (ASTail), and a mixture of DPPC and DPPE. The differences in the calculated PMFs for the various systems are presented, and arguments are made for the fusogenicity of the various lipid systems. The overall energetics associated with the initiation of the fusion process is connected with the lipid dynamics by an analysis of the local molecular conformations involved in these initial events.

The focus of this work is on the free energy path that yields initial mixing of lipids. From theoretical models, this is the largest barrier on the path to a single, fused vesicle.^{7,8} At least one additional barrier exists further along the path to full fusion, has been observed in our previous simulations,¹⁶ and was characterized in the works of Kasson et al.^{9,18} In this work, we calculate the initial free energy barrier of lipid mixing and examine the lipid dynamics involved in the initial mixing process.

Methods

System Setup and Molecular Dynamics Simulation. We used the coarse-grained force field developed by Marrink et al. for lipids.²⁴ The initial coordinates of an individual DPPC vesicle were based on previously self-assembled configurations. Each vesicle has 877 lipids. The DPPC system had 129 492 coarse-grained water particles. Vesicle diameters are given in Table 1.

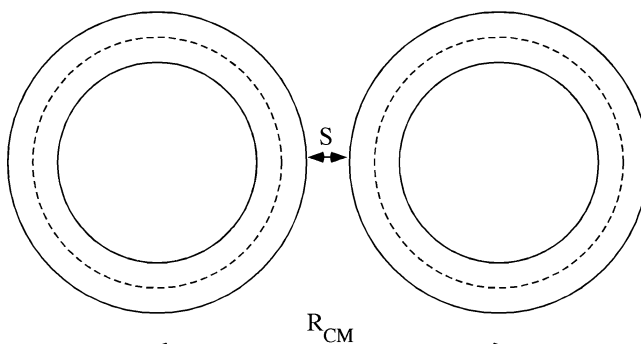


Figure 1. A schematic of two vesicles restrained at a center of mass separation of R_{CM} . The distance S represents the surface separation, which has more than one definition, as discussed in the text.

A mixed DPPC/DPPE (3:1) vesicle was created from an equilibrated system of DPPC vesicles following the distribution of PE and PC lipids in the inner and outer monolayers as determined by Marrink and co-workers.²⁵ The vesicles with asymmetric lipid tails (ASTail) were created by removing two of the four beads from one of the aliphatic tails of each lipid of the equilibrated DPPC/DPPE system. A DOPC vesicle was constructed starting from the coordinates of a POPE vesicle.²⁵ An additional bead was attached to the shorter tail of the POPE lipids, and the system was pre-equilibrated by first using the LAMMPS soft cosine potential to push apart overlapping particles. This was followed by incrementally increasing the 1–3 interactions in the system from zero to full strength under NPT conditions using the complete potential of the force field for DOPC lipids.

All simulations were performed with the LAMMPS simulation package.²⁶ A time step of 30 fs was employed during the equilibration runs. Each double vesicle system was equilibrated in the constant NPT ensemble (325 K and 1 atm) for 100 ns, using a Nose–Hoover thermostat and barostat.²⁷ An equilibrated state of the system of two DPPC vesicles had dimensions of 222.7 Å × 222.7 Å × 375.1 Å. The time scales presented here are simulation times without any scaling factors.

Umbrella Sampling Simulations. For the umbrella sampling simulations, the reaction coordinate was chosen to be the distance between the center of mass (R_{CM}) of the two vesicles in the system (Figure 1). A harmonic umbrella potential with a force constant of 150.0 kcal mol⁻¹ Å⁻² was applied. For the two DPPC vesicle system, 33 windows were sampled spanning the vesicle–vesicle CM separations from 143.7 to 135.7 Å. In general, to achieve sufficient sampling, the spacing between windows was between 0.2 and 0.3 Å. The number of windows sampled in each system varied depending on the range of CM distances sampled. Thirty-four windows were sampled for the DPPC/DPPE system; 114 windows, for asymmetric; and 164 windows, for DOPC. The production simulations were for 90 ns per window using the same NPT conditions under which the systems were equilibrated. The PMF profile was generated using the weighted histogram analysis method using the implementation of Grossfield.²⁸

The focus here is on the free energy of the initial fusion events and its dependence on the lipid type. The PMFs were calculated for shorter and shorter separations until the mixing of the outer leaflets occurred. Calculations of the PMF beyond this point require more sophisticated and demanding constraint methods that are appropriate for future work. A more detailed sampling of the full free energy path would round off our calculated curves of the initial fusion barrier. From the data analysis, we

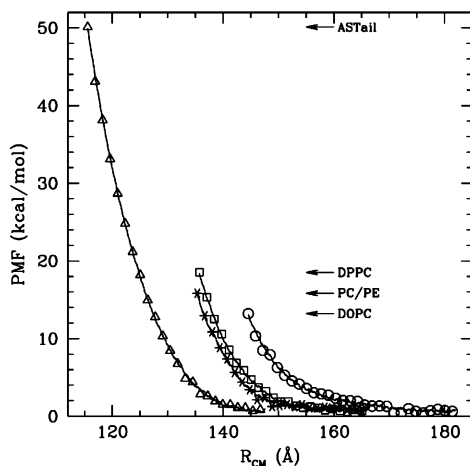


Figure 2. A plot of the PMF as a function of the constrained center of mass distance (R_{CM}) for the systems with DPPC (\square), PC/PE (*), DOPC (\circ), and ASTail (Δ) vesicles. The lines of all four data sets represent the raw PMF data without any smooth fitting. Arrows indicate the free energy values where fusion initiation occurs (where curves end).

TABLE 2: PMF Values at Initial Fusion (kcal/mol) and the Center of Mass Separation Distance (R_{CM}) at Fusion^a

	DPPC	PC/PE	DOPC	ASTail
PMF(kcal/mol)	18.5	15.8	13.2	50.1
R_{CM}	135.5	135.0	144.3	115.3
S_h	6.5	6.0	8.5	-4.7
S_f	3.0	4.0	6.3	-6.7

^a S is the distance of closest approach for the vesicle surfaces. Distances are in Å.

know that this will affect only the final angstrom or so of data and not depend on the lipids type. The dynamics in the simulations did progress beyond the initial formation of the hydrophobic core. All systems generally followed the progression to fusion once the stalklike hydrophobic pore had been formed: initially proceeding to a hemifused state and subsequently to complete fusion. For example, in one case, once a hydrophobic pore had been formed between two DPPC/DPPE vesicles, the system proceeded to complete fusion in an additional 13 ns of simulation.

Results

The Free Energy Barrier. For each lipid type, the PMFs are shown as a function of the center of mass separation distance, R_{CM} , in Figure 2. The largest separation was chosen so that the slope of each PMF curve reaches zero at large R_{CM} . As the vesicle separation decreases, the PMF rises monotonically in all cases. The point where the curves end is the separation distance at which fusion initiation occurs; that is, the mixing of lipids between the two vesicles. A more detailed description of these events for each system will be given in the next subsection. In the following discussion, “fusion” will refer to this initial mixing of lipids, which is the first critical event in the sequence of states that ultimately leads to a single, fused vesicle. The separation distances just before the fusion by mixing of the outer leaflets and the PMF values at this position are given in Table 2. These values are taken to be the barrier energies for fusion initiation. Three of the lipid systems have maximum PMF values of ~ 15 kcal/mol. The barrier for the DPPC system is ~ 5 kcal/mol larger than the value for the DOPC system. The most dramatic difference among the four system occurs for the ASTail

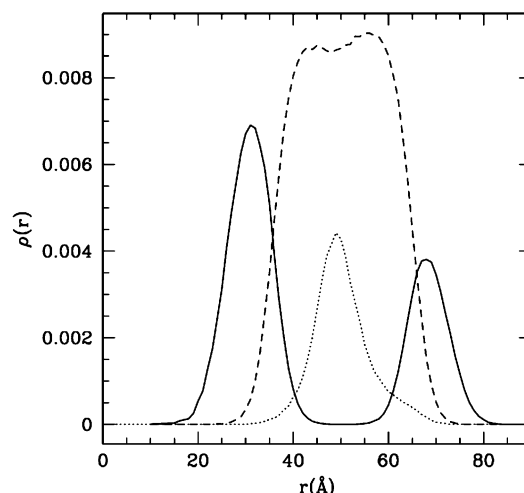


Figure 3. Radial density profile for the DOPC system with the origin at the vesicle center of mass. The solid lines are the headgroup density, the dashed line is the tail group density, and the dotted line is the tail ends.

system, which has a fusion initiation barrier of 50 kcal/mol. The value of R_{CM} at fusion varies considerably. The value for the DOPC system is at much larger R_{CM} because the diameter of the DOPC vesicle is larger than the others (see Table 1). The larger diameter is a consequence of the larger area/lipid and thickness due to the unsaturated DOPC tails and slightly longer DOPC tails in comparison to DPPC. The vesicles with asymmetric tails have a smaller diameter and correspondingly smaller value of R_{CM} at fusion, which is ~ 20 Å closer than the other systems.

Given that the vesicle size is so important, it is reasonable to consider scaling its dependence from the PMF curves. The key distance for fusion is more appropriately the surface separation, where $S = R_{CM} - D$, and D is the vesicle diameter. To calculate the vesicle diameter, we first use the radial density profiles of the vesicles. Figure 3 shows the radial density profiles with the head, tail, and tail-end densities individually plotted for DOPC. Because these are *radial* densities, they are not symmetric, like planar lipid bilayer profiles. Otherwise, the two headgroup peaks are present with the tail group distribution between them. The value of the diameter, D_h , in Table 1 was calculated using the outer headgroup peak positions of the radial densities. For later discussion, we note that the tail end density within the outer headgroup region is nonzero. Otherwise, the tail ends have a narrower distribution, which is peaked in the middle, as expected.

In Figure 4, we plot the PMF as a function of the normalized separation, $S_f = (R_{CM} - D_f)/D_f$, where D_f is the diameter value that gives the best overlap of curves in Figure 4. The initial estimate for D_f was D_h , and it was then adjusted. The values of D_f used in Figure 4 are listed in Table 1 and are about equal to $D_h + 3$ Å. We note that slight (1 Å) variations about this value produce a markedly better overlap. Physically, D_f is a better measure than D_h of the outer surface where contact occurs. On the other hand, as will be shown, the vesicles deform and the actual surface separation varies as a function of R_{CM} . S_f is then a measure of the surface separation between unperturbed vesicles.

The scaled plot shows that all the data lie on the same curve. The ASTail case extends to higher PMF values, since fusion does not occur until much shorter separations. The overlap of the different systems indicates that the barrier energy has the same sources. The two main dynamical elements are the removal

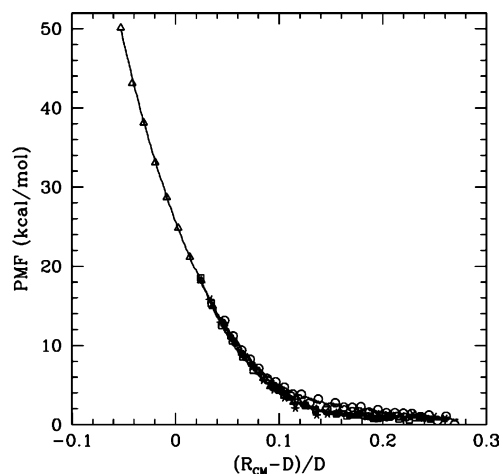


Figure 4. A plot of the PMF as a function of the center of mass separation scaled by the vesicle diameter for the same systems as in Figure 2, where the diameter of the fit value is given in Table 2.

of the water between the vesicles and the deformation of the vesicle. More water must be removed for fusion of the ASTail system, which raises its free energy barrier to higher values relative to the other systems. The flexibility of the bilayer determines the cost of the vesicle deformations.

In calculating the surface separation between the vesicles, it is clear that the vesicles become deformed with decreasing R_{CM} . The degree of deformation can be measured by considering the deviation from the original spherical geometry of the two vesicles. In Table 2, we list the two sets of $S = R_{CM} - D$, which measures the surface separation between the vesicles. The values of D_h and D_f that are used to calculate the corresponding values of S are given in Table 1. Except for the ASTail system, the S_h and S_f are positive, which implies that the peaks of headgroup distribution do not overlap. However, it is clear that part of the headgroup distribution implies overlap. In fact, if we calculate the separation distance $R_{CM} - D_o$, we obtain negative values for all systems. This contrasts with the images shown below that have a water gap between the vesicles. Since the values for D_h come from radial averages, the actual lack of overlap implies that the vesicles have deformed and the spherically averaged distributions do not yield good measures of the surface separation.

To obtain a better measure of the surface separation, we have also calculated density distributions binned along the axis that is coincident with the center of mass separation. These distributions give a more direct measure of the surface separation as the two vesicles are brought together. The deformation is asymmetric in that the near sides of the vesicles that ultimately fuse are slightly flattened. Especially for the ASTail system, the degree of compression on the contact side is noticeable in the distributions. Since these are distributions that include the fluctuations of the lipid dynamics, we need to define how to calculate the separation distance. We set the separation distance to be the distance between the positions of the half height of each outer headgroup distribution's shoulder. This effectively gives the average separation of the outer, facing leaflets. For the DOPC, DPPC, and ASTail systems, the separation values just before fusion are $S = 10.5, 8.5$, and 6.5 \AA , respectively. The longer lipids have the larger separations. The magnitude of these separations is consistent with the images below concerning the amount of water between the vesicles just before fusion.

Conformational Dynamics of Fusion Initiation. The dynamics of the initial lipids that cross from one vesicle to another

can be explicitly examined graphically in the simulations. We will now discuss the lipid dynamics for each of the four systems. We have examined the lipid dynamics for a range of times near the fusion event. Only images of the first complete connection between the two vesicles are shown in the figures. Details of the dynamics before and after are discussed in the following text.

An image of the initial fusion event for the DPPC system at $R_{CM} = 135.5 \text{ \AA}$ is shown in Figure 5a. A single lipid with splayed tails spans the distance between the two vesicles and connects the two vesicles. Examination of subsequent frames of the simulation show that rather quickly, another lipid tail moves along the splayed lipid tail and begins the formation of a hydrophobic pore and subsequently the fusion stalk. The splay geometry allows a single lipid to make the connection between the two vesicles. The separation distance between the tail ends determines the possible spanning distance and the maximum vesicle separation. To get a better idea of the possible range of tail end separations, we calculated the distribution of separation distances between the two tail end beads for the two vesicles at the largest separation (i.e., unperturbed vesicles). The largest peak in the distribution occurs at the separation corresponding to contact between the tails. A secondary peak occurs for a separation corresponding to the tail bead of another lipid between the two ends. At larger separations, the distribution monotonically decreases. The maximum tail end separation is 39.6 \AA . The fraction of separations $>20 \text{ \AA}$ is 0.18; thus, there are a substantial number of strongly splayed lipids within the vesicle.

The image of the initial fusion for the ASTail system is especially revealing for understanding an important aspect of the molecular basis of the fusion event. Figure 5b shows a single splayed lipid that spans the two vesicles, such as the DPPC case in Figure 5a. However, in the ASTail case, the shorter tail requires a smaller separation of the vesicles before fusion can occur. From the images, it is clear that the thickness of the water region between the vesicles is only one or two water beads wide. Thus, there are two critical components of the mechanism for fusion initiation. First, tail splay enables a single tail to enter the water barrier region at half the cost of two tails' crossing. Second, as these results show, spanning the separation between the fusing vesicles is critical, and the range of separation distances between splayed tail ends influences the fusion statistics. For this reason, asymmetric tail lengths do not promote fusion more than symmetric tails. In fact, asymmetric tails inhibit fusion. Experimentally, this has been known for some time.²⁹

In the DOPC system, we observe multiple failed attempts of lipids to cross from one vesicle to another at the fusion separation distance. In these attempts, the tails enter the water region between the vesicles but do not connect the two vesicles, and the tails return to their respective vesicle. Subsequently, a single lipid with splayed tails is able to enter the hydrophilic interstitial region (Figure 5c) and reach the opposite vesicle to form a bridge between the two vesicles. This event spawns the hydrophobic pore formation by enabling other lipids to enter the hydrophilic region at a reduced free energy cost by keeping their tails close to the splayed lipid's tails. The stalk formation quickly follows. This shows that after an initial splayed tail enters the interface, subsequent tail insertions can add to that initial event.

A variation of the above lipid dynamics is seen in the DPPC/DPPE image (Figure 6a). In this case, two lipids make the initial contact between two vesicles. One of these lipids is splayed with a tail in the hydrophilic region between the vesicles (Figure

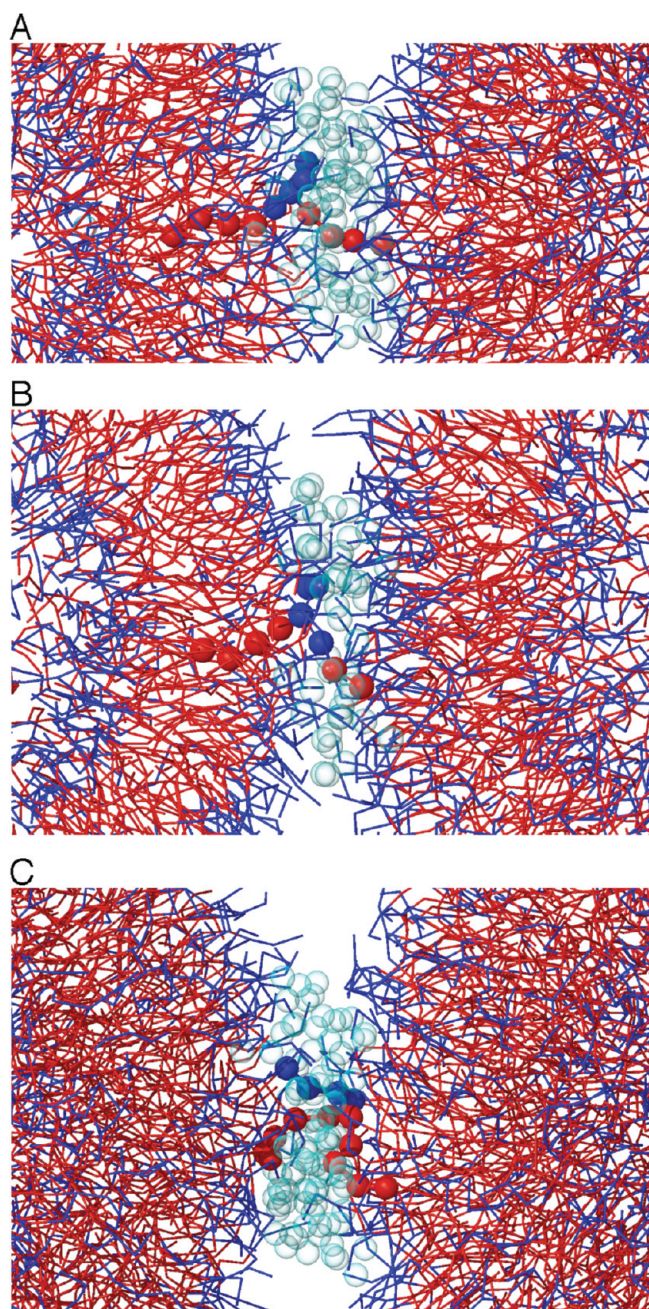


Figure 5. Lipid conformations during initial formation of the hydrophobic pore before fusion. Lipids are generally shown in stick representation. Individual lipids that cross from one vesicle to the other to form the hydrophobic pore are shown in ball and stick representation. In all cases, the headgroup bonds and beads are blue, and the tail group bonds and beads are red. Water beads near the lipids crossing between vesicles are shown in transparent cyan. (a) A single lipid in a splay conformation between two DPPC vesicles at $R_{CM} = 135.5 \text{ \AA}$ after 16.6 ns of simulation. (b) In the ASTail system, a single lipid with tails splayed spans the vesicles at $R_{CM} = 115.3 \text{ \AA}$ after 12.8 ns of simulation. (c) In the DOPC system at $R_{CM} = 144.3 \text{ \AA}$ after 53 ns of simulation, a single lipid with tails splayed spans the two vesicles.

6b), and a second lipid has a tail next to the splayed lipid, but its tail is not splayed (Figure 6c). The head groups of both lipids extend toward the apposing vesicle. This combination forms a bridge between the two vesicles.

In all the lipids systems studied, we find that lipid splay plays a central role in initiating the breakdown of the hydrophilic barrier and starting the connection between the two vesicles. Once one lipid has performed this function, then other lipids

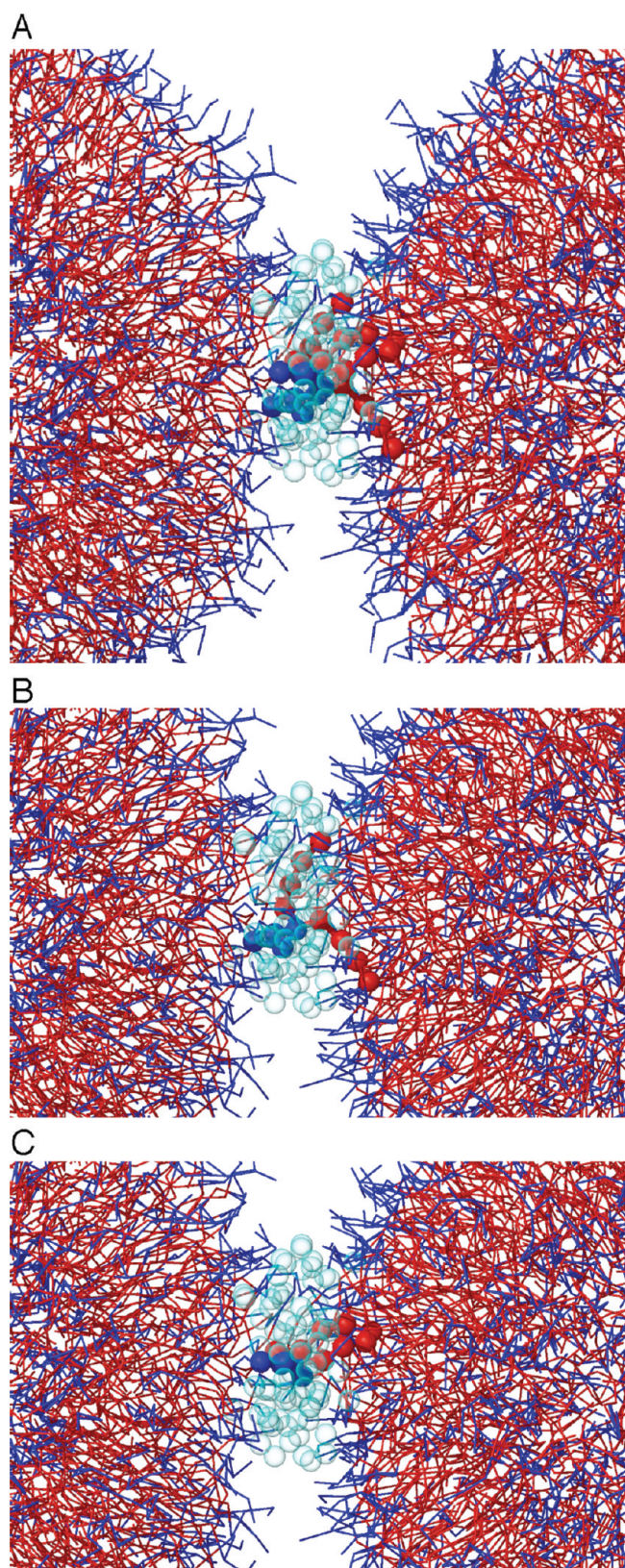


Figure 6. (a) Two lipids initiate the fusion in the PC/PE system. (b) One of the (PE) lipids has splayed tails and (c) the second (PC) lipid is “translated” directly across with one of its tails next to one of the splayed lipid’s tail. The hydrophobic pore is formed at $R_{CM} = 135.0 \text{ \AA}$ after 23.0 ns of simulation. Visualization representations are the same as in Figure 5.

can follow by positioning their tails next to the splayed lipid’s tails. In this manner, a hydrophobic region forms within the

hydrophilic region between the vesicles, and subsequently, the outer leaflets will fuse.

Discussion

In this work, we have studied fusion between vesicles with varying lipid type. In comparison with our original work, we use more advanced coarse-grained lipid models to treat the different lipid types and find the role of lipid tail splay to be even more important than originally thought.¹⁶ Below, we discuss the dynamics of tail splay and the important geometric factors that are involved in the initial fusion event. These factors determine the relative impact of different lipid tails on the energy landscape. We show that the dynamics of the tail ends is critical and is correlated with the fusogenicity of the lipids. We discuss the reduction in the barrier height and compare our calculations of the free energy barrier with that of other calculations.

The Role of Aliphatic Tail Splay. In this set of simulations, we find that splayed tails are involved in the fusion initiation in every case. These results are a confirmation and an expansion of our earlier study, which used a more simplified coarse-grained model.¹⁶ This suggests that there are dominant energetic reasons for splay to occur. Another vesicle simulation has also observed splay in fusion initiation,¹⁷ and the findings of recent simulation have concluded that splay plays an important role in fusion.¹¹ Splay conformations have also been observed experimentally in the formation of an initial hydrophobic pore for fusion.³⁰ Energetically, lipid splay has an advantage: the cost of introducing one tail versus two tails into the hydrophilic region is reduced by a factor of 2. In addition, the separation distance between vesicles at fusion is larger, which reduces the cost of water confinement. An unsplayed lipid can connect only the headgroup of the opposite vesicle to the tail region of its vesicle, which forces the gap between the vesicles to be small. In addition, a splayed lipid connects the tail regions of the outer leaflets of both vesicles allowing lipids from *both* vesicles to move along the splayed lipid to the opposite vesicle. Thus, the splayed lipid more readily promotes the fusion stalk formation. For these reasons, the initial splayed event and the association of splayed tails is the key molecular mechanism for initiation of fusion.

We believe it is important to emphasize that the splay mechanism can initiate fusion without the vesicles' being in contact; that is, there remains a gap containing water between the vesicles when fusion occurs. Although this gap is only a few water molecules thick, the cost is very steep for removing additional waters.³¹ Thus, the barrier is substantially lowered by not having to remove water molecules near the vesicles. This is clearly displayed in the ASTail system, which has the highest barrier of the systems studied and the smallest gap separation. The point is further made by the fact that in Figure 4, the ASTail free energy curve overlays the DOPC curve, implying that the additional cost of removing the waters for the ASTail system is the source of the free energy increase.

For splay to play a role in fusion, the lipid tail end must spend time in the headgroup region. For well-separated vesicles, we have calculated the distribution of the minimum separation between each tail end bead and any water outside the vesicle (Figure 7). The minimum distance between a point and a set is a well-defined metric. In this case, the set is all the waters external to the vesicle. For each tail end, we obtain the closest separation to the external waters, which is the physically desired distance. The distribution was normalized such that the sum over the bins equals one. From these distributions, we determined the fraction of tail ends in contact with the external water,

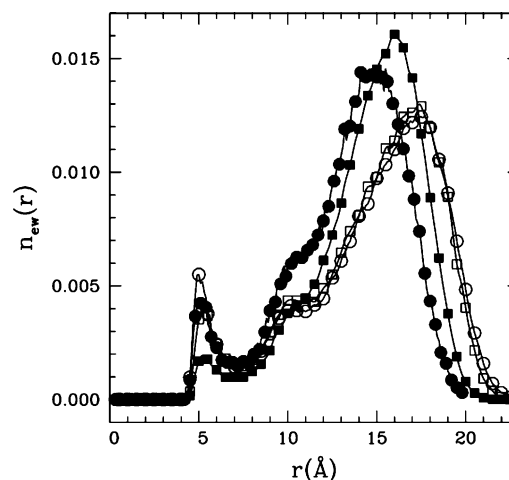


Figure 7. Distributions of the tail end distance from external water molecules for planar DPPC (■), vesicle DPPC (●), planar DOPC (□) and DOPC vesicle (○).

where we defined contact to be the fraction within the first peak that extends to $r = 6.8 \text{ \AA}$, the minimum position of the trough. For DPPC, the contact fraction is 0.064, and for DOPC it is 0.075. The larger fraction for DOPC is consistent with the lower free energy barrier for DOPC.

In the overall distributions shown in Figure 7, the main difference between DOPC and DPPC is due to the different lengths of the chains, which affects the distribution at large r values and does not impact the contact with water. We have also calculated the fraction of tail ends in contact with water for planar bilayers because we expected to see a stronger difference between DPPC and DOPC for this geometry, and the planar geometry is the large (i.e., infinite) diameter limit, which will indicate the effect of increasing vesicle size. Due to the packing of the saturated tails of DPPC, we expected the DPPC tail ends would have a lower probability of water contact than DOPC tail ends in the planar geometry. The calculated water contact fraction demonstrates this difference: in a planar bilayer, the fraction is 0.031 for DPPC and 0.061 for DOPC. Thus, there is a factor of 2 drop for planar DPPC system as compared with DOPC. Since the contact of the tail ends with water is lower in the planar geometry, the data indicate that fusion initiation events will be more likely to occur in DPPC vesicles than in DPPC planar bilayers. This is consistent with the lack of fusion between DPPC GUVs. The tiny DPPC vesicles treated in this work are significantly different from larger vesicles or a planar bilayer and can fuse. The contact difference between vesicle and planar geometries for DOPC is 0.014, which is half of the difference for DPPC. This indicates that there would be a difference in the fusion rate between large and small vesicles of DOPC, but this difference would not be as big as for DPPC. This is in agreement with experimental data.^{32,33}

With respect to the overall fusion frequency we note that for fusion to occur, tail splay must occur in a lipid in the "contact" region of the two vesicles. This requires a correlated set of events. First, there must be lipid tail splay. Second, one tail must enter the hydrophilic region. Third, the tail must enter the water in the regime between the two vesicles. For the small vesicles treated here, the fusion rates are rather fast. Reducing any of these factors reduces the fusion rate. In addition, with respect to the measured fusion frequency, the time scales in the simulations are much shorter than in experiments, because the simulations do not include the (slow) time for vesicles to

diffuse and collide. The center of mass distance constraint starts the vesicles close together and keeps the “collision” aligned promoting fusion. Thus, a substantial time for fusion must be added to the simulation times to replicate the experimental conditions, which will depend on vesicle concentration, among other quantities.

Free Energy Barrier to Liposome Fusion. Our calculations yield barrier heights in the range of 13–18 kcal/mol, except for the asymmetric tail length lipids, which have a large barrier of 50 kcal/mol. We have discussed why the free energy barrier is so much higher for the asymmetric case. Since the PMF curve is coincident for all of the systems, the same contributions to the barrier exist for all cases. The two main contributions are the removal and confinement of water between the two vesicles and the deformation of the vesicles upon approach. The bending modulus of the DPPC coarse-grained model is in agreement with experimental values.³⁴ The difference in measured values of the bending modulus between DPPC and DOPC is, at most, a factor of 2.²² This difference is not expected to result in a large difference in the deformation energy for the small deformations observed in these two systems. Moreover, for the small vesicles studied here, the bending moduli may be even closer in value due to vesicle geometry dominating over lipid composition. Thus, we expect that water removal is the primary free energy cost. Testing this hypothesis will be part of future work. We next compare our calculated free energy barrier to other calculations, particularly for the DOPC system.

Kuzmin et al. introduced a modified stalk geometry and calculated the free energy barrier to be 22 kcal/mol.⁷ This calculation is for parallel planar membranes in which apposed nipples of radius 8 nm fuse together. Thus, the local curvature is close to what has been simulated in this work, although the overall geometry is different. Kozlovsky and Kozlov performed a calculation including additional degrees of freedom in the lipid orientation and calculated a free energy barrier for DOPC to be 27 kcal/mol.⁸ Their starting geometry is similar to that used by Kuzmin et al. The separation of the bilayer is 15 nm, corresponding to protrusions of radius 7.5 nm. The lateral curvature radius is larger and is 20 nm for the given free energy value. Our barrier height for DOPC is lower than these calculated values. The splay of the lipid tails is not included in these calculations. Given that all other components of the free energy are included in both calculations, we expect the barrier to be smaller in the simulations. The magnitude of the difference is significant (8–13 kcal/mol) and is in a range to be expected for the physical mechanism. Knecht and colleagues have also examined the fusion between two flat bilayers using a coarse grained model and identified a barrier of $20k_B T$.¹¹ However, their approach was to compute the free energy as a lipid in one bilayer was displaced from its initial position across the gap between the membranes. The relevance of the lipid displacement energetics they identify to actual fusion is uncertain, and it is difficult to compare the values they obtain with those found here.

Using a DPD model of lipids in simulations of fusion between a vesicle and a plane, Grafmüller et al. found a barrier of 6 kcal/mol.¹² DPD models are more weakly interacting and allow particles to pass through each other. Consequently, the barriers are expected to be lower. In fact, Kasson et al. found no fusion between a vesicle and a planar bilayer in their molecular dynamics simulations using the Marrink coarse-grained lipid model that we used.¹⁸ The recent simulations by Smirnova et al. did not find fusion in simulations of low hydration between two planar bilayers (until they perturbed the system by pulling

a lipid from one bilayer to the other).¹¹ We note that we also attempted fusion between a vesicle and a bilayer and did not observe fusion. For these reasons, we believe the DPD calculations to significantly underestimate the free energy barrier. We also note that Katsov et al. calculated a 6 kcal/mol free energy barrier, but their calculation was for a polymeric diblock system.³⁵ Although such a system will behave qualitatively similarly to the lipid system, the energetics are not expected to be the same, and direct comparison with lipid systems should not be done at this level.

We originally started this study using the new MARTINI force field,²¹ but we were unable to observe fusion up to barriers >100 kcal/mol. We determined that the source of this was the value for σ between tail and head or water beads, which was increased from 4.7 to 6.2 Å in the MARTINI force field. The large cross term for σ is inconsistent with the much smaller σ values of the CG particles. At the time, we were uncomfortable with independently adjusting this parameter and used the original version of the force field. In subsequent conversations with Marrink, he agreed that this larger value of σ has the effect that we observed and suggested using the original value of σ . We have performed simulations for the DOPC system with the “revised” MARTINI force field and obtain the same free energy curve within the uncertainty of the data. Thus, we are comfortable with the results presented in this paper and know that the results do not change significantly using the revised MARTINI force field. In this paper, we focus on the presentation of the results of the simulations and do not discuss the details of force fields, which while computationally interesting are in the end not significant. A separate paper will discuss free energy of fusion calculations for different coarse-grained force fields.

Vesicle Size Dependence. The fusion between large (100–200 nm) unilamellar vesicles of DPPC and even DOPC has not been observed.³³ This raises questions concerning the results of these simulations. The simulations presented here are for very small vesicles, and experiments on small unilamellar vesicles (40 nm diameter) do observe fusion, albeit very slowly.³² Even this diameter is large compared with the simulation vesicles. The smaller vesicles have larger curvature effects, producing substantial effects on the fusion time. Kasson and Pande simulated fusion between POPC vesicles for two diameters and found the dynamics to be much slower for the 19 nm vesicles than the 15 nm vesicles. There is likely to be more strain within the bilayer of the smaller vesicles, which can be relieved by fusion. In other words, there is more to gain in free energy by fusion for tiny vesicles. The initial fusion dynamics is promoted by the lipid tails in the outer leaflet of small vesicles being more exposed to water. As discussed above, there is a significant difference in the fraction of tail ends that make contact with external waters between planar and small vesicles, as well as between DPPC and DOPC vesicles. This result is consistent with the experimental observation that larger vesicles have lower fusion rates and that DOPC is more fusogenic than DPPC.^{33,36} The fact that in the tiny vesicles the DPPC and DOPC contact fractions are closer than in planar geometries suggests that the small diameter alters the situation promoting fusion in DPPC. Clearly, the size dependence of vesicle fusion is an area of further investigation.

Conclusion

We have performed molecular dynamics simulations to characterize the free energy barrier for the fusion of two vesicles and to examine the molecular details of barrier crossing. The simulations studied fusion between two vesicles of the same composition. Three systems consisted of a single lipid type,

DPPC, DOPC, and a lipid (ASTail) with asymmetric tail lengths (one tail of DPPC was reduced to half the length), and one system was a 3:1 DPPC/DPPE mixture. The relative barrier heights for these systems was found to be ASTail \gg DPPC > DPPC/DPPE > DOPC, in agreement with experimental observations. DOPC vesicles have the lowest free energy barrier of 13.2 kcal/mol. The DPPC vesicles have a 5.3 kcal/mol larger barrier. The asymmetrical tail system has a prohibitively large barrier (50.1 kcal/mol), consistent with the fact that lysolipids are fusion demoters. In all cases, we find that splay of the lipid tails is the conformational feature involved in the initiation of fusion. In fact, typically, we find a single lipid initiates fusion by splaying and spanning between the two vesicles. This mechanism reduces the free energy cost from that calculated solely on membrane bending and hydration costs.⁷ In addition to the free energy advantage of a single tail crossing the hydrophilic region in comparison to two tails, there are other important advantages of splay. A single splayed lipid can span the separation between the vesicles with a greater separation than unsplayed lipids. This reduces the amount of water that must be removed between the vesicles before fusion occurs lowering the free energy barrier. This effect is exhibited clearly by the vesicles composed of lipids with asymmetric tails that have a much higher fusion barrier than the other systems because the shorter tail has a shorter spanning distance. For lipid tails to splay and initiate fusion, contact of the tail end with the external waters is necessary. We have found that DPPC and DOPC bilayers differ in the fraction of lipids that contact water, especially in planar lipid bilayers. This result indicates why DPPC has such a low fusogenicity. In general, the tail end distribution plays an important role in determining fusogenicity of lipids.

Acknowledgment. This work was funded by NIH NIGMS Grant 5R21GM076443 and was performed, in part, at the Center for Integrated Nanotechnologies, a U.S. Department of Energy, Office of Basic Energy Sciences user facility. Sandia National Laboratories is a multiprogram laboratory operated by Sandia Corporation, a Lockheed-Martin Company, for the U.S. Department of Energy under Contract No. DE-AC04-94AL85000.

References and Notes

- (1) Finger, F. P.; White, J. G. *Cell* **2002**, *108*, 727.
- (2) Jahn, R.; Südhof, T. C. *Annu. Rev. Biochem.* **1999**, *68*, 863.
- (3) Mercer, J.; Knebel, S.; Schmidt, F. I.; Crouse, J.; Burkard, C.; Helenius, A. *Proc. Natl. Acad. Sci. U.S.A.* **2010**, *107*, 9346.
- (4) Chernomordik, L. V.; Kozlov, M. M.; Zimmerberg, J. *J. Membr. Biol.* **1995**, *146*, 1.
- (5) Jesorka, A.; Orwar, O. *Ann. Rev. Anal. Chem.* **2008**, *1*, 801.
- (6) Markin, V. S.; Kozlov, M. M.; Borovjagin, V. L. *Gen. Physiol. Biophys.* **1984**, *3*, 361.
- (7) Kuzmin, P. I.; Zimmerberg, J.; Chizmadzhev, Y. A.; Cohen, F. S. *Proc. Natl. Acad. Sci. U.S.A.* **2001**, *98*, 7235.
- (8) Kozlovsky, Y.; Kozlov, M. M. *Biophys. J.* **2002**, *82*, 882.
- (9) Kasson, P. M.; Kelley, N. W.; Singh, N.; Vrljic, M.; Brunger, A. T.; Pande, V. S. *Proc. Natl. Acad. Sci. U.S.A.* **2006**, *103*, 11916.
- (10) Norizoe, Y.; Daoulas, K. C.; Muller, M. *Faraday Discuss.* **2010**, *144*, 369.
- (11) Smirnova, Y. G.; Marrink, S. J.; Lipowsky, R.; Knecht, V. *J. Am. Chem. Soc.* **2010**, *132*, 6710.
- (12) Grafmuller, A.; Shillcock, J.; Lipowsky, R. *Phys. Rev. Lett.* **2007**, *98*.
- (13) Shillcock, J. C.; Lipowsky, R. *Nat. Mater.* **2005**, *4*, 225.
- (14) Noguchi, H.; Takasu, M. *J. Chem. Phys.* **2001**, *115*, 9547.
- (15) Marrink, S. J.; Mark, A. E. *J. Am. Chem. Soc.* **2003**, *125*, 11144.
- (16) Stevens, M. J.; Hoh, J. H.; Woolf, T. B. *Phys. Rev. Lett.* **2003**, *91*, 188102.
- (17) Smeijers, A. F.; Markvoort, A. J.; Piteerse, K.; Hilbers, P. A. J. *Phys. Chem. B* **2006**, *110*, 13212.
- (18) Kasson, P. M.; Pande, V. S. *PLoS Comput. Biol.* **2007**, *3*, 2228.
- (19) Goetz; Lipowsky, R. *J. Chem. Phys.* **1998**, *108*, 7397.
- (20) Stevens, M. J. *J. Chem. Phys.* **2004**, *121*, 11942.
- (21) Marrink, S. J.; Risselada, H. J.; Yefimov, S.; Tieleman, D. P.; de Vries, A. H. *J. Phys. Chem. B* **2007**, *111*, 7812.
- (22) Orsi, M.; Michel, J.; Essex, J. W. *J. Phys.: Condens. Matter* **2010**, *22*, 155106.
- (23) *Coarse-Graining of Condensed Phase and Biomolecular Systems*; Voth, G., Ed.; CRC Press: Boca Raton, 2008.
- (24) Marrink, S. J.; de Vries, A. H.; Mark, A. E. *J. Phys. Chem. B* **2004**, *108*, 750.
- (25) Marrink, S. J.; Mark, A. E. *J. Am. Chem. Soc.* **2003**, *125*, 15233.
- (26) Plimpton, S. *J. J. Comput. Phys.* **1995**, *117*, 1.
- (27) Martyna, G. J.; Tobias, D. J.; Klein, M. L. *J. Chem. Phys.* **1994**, *101*, 4177.
- (28) Kumar, S.; Rosenberg, J. M.; Bouzida, D.; Swendsen, R. H.; Kollman, P. *J. Comput. Chem.* **1992**, *13*, 1011.
- (29) Chernomordik, L. V.; Kozlov, M. M.; Melikyan, G. B.; Abidor, I. G.; Markin, V. S.; Chizmadzhev, Y. A. *Biochim. Biophys. Acta* **1985**, *812*, 643.
- (30) Holopainen, J. M.; Lehtonen, J. Y. A.; Kinnunen, P. K. J. *Biophys. J.* **1999**, *76*, 2111.
- (31) Rand, R. P.; Parsegian, V. A. *Biochim. Biophys. Acta* **1989**, *988*, 351.
- (32) Lentz, B. R. *Eur. Biophys. J.* **2007**, *36*, 315.
- (33) Burgess, S. W.; Massenburg, D.; Yates, J.; Lentz, B. R. *Biochemistry* **1991**, *30*, 4193.
- (34) de Vries, A. H.; Mark, A. E.; Marrink, S. J. *J. Phys. Chem. B* **2004**, *108*, 2454.
- (35) Katsov, K.; Müller, M.; Schick, M. *Biophys. J.* **2004**, *87*, 3277.
- (36) Lentz, B. R.; Carpenter, T. J.; Alford, D. R. *Biochemistry* **1987**, *26*, 5389.

JP1055182